Kinetically distinct phases of tau on microtubules regulate kinesin motors and severing enzymes

Valerie Siahaan[1,5], Jochen Krattenmacher [1,5], Anthony A. Hyman[2,3,6], Stefan Diez [2,3,4,6], Amayra Hernández-Vega [2,6*], Zdenek Lansky [1,6*] and Marcus Braun [1,4,6*]

Tau is an intrinsically disordered protein, which diffuses on microtubules[1]. In neurodegenerative diseases, collectively termed tauopathies, malfunction of tau and its detachment from axonal microtubules are correlated with axonal degeneration[2]. Tau can protect microtubules from microtubule-degrading enzymes such as katanin[3]. However, how tau carries out this regulatory function is still unclear. Here, using in vitro reconstitution, we show that tau molecules on microtubules cooperatively form cohesive islands that are kinetically distinct from tau molecules that individually diffuse on microtubules. Dependent on the tau concentration in solution, the islands reversibly grow or shrink by addition or release of tau molecules at their boundaries. Shielding microtubules from kinesin-1 motors and katanin, the islands exhibit regulatory qualities distinct from a comparably dense layer of diffusible tau. Superprocessive kinesin-8 motors penetrate the islands and cause their disassembly. Our results reveal a microtubule-dependent phase of tau that constitutes an adaptable protective layer on the microtubule surface. We anticipate that other intrinsically disordered axonal proteins display a similar cooperative behaviour and potentially compete with tau in regulating access to the microtubule surface.

Tau is an intrinsically disordered microtubule-associated protein (MAP), which localizes preferentially to neuronal axons and is involved in neurodegenerative diseases[4–6]. Tau enhances the stability of microtubules directly by its presence[7], and by regulating the interactions of other MAPs with microtubules[8–13]. Tau mislocalization during the onset of Alzheimer's disease leaves axonal microtubules unprotected against microtubule-severing enzymes such as katanin[3], leading to microtubule destabilization and the eventual degeneration of the axon. The molecular mechanism underlying this regulatory function of tau is unknown. Here we demonstrate how microtubule-associated tau molecules can collectively regulate molecular motors and severing enzymes.

To study microtubule-associated tau molecules, we immobilized Atto 647-labelled microtubules on a coverslip, added full-length, human tau 441 isoform (encoded by 2N4R), fluorescently labelled on the C terminus with either monomeric enhanced green fluorescent protein (tau–meGFP) or mCherry (tau–mCherry) and performed time-lapse imaging using total internal reflection fluorescence (TIRF) microscopy (Fig. 1a and Methods). After the addition of 20 nM tau–meGFP, we observed the formation of high-density tau–meGFP islands on the microtubules, surrounded by regions of low-density

tau–meGFP (Fig. 1b–d and Supplementary Video 1). Tau–meGFP islands originated from diffraction-limited spots, appearing within tens of seconds after the addition of tau (Supplementary Fig. 1a). The islands grew intermittently at their boundaries with variable velocities in the order of 25 nm s^{-1}, corresponding to about 10 molecules added per s (Supplementary Fig. 1b) to highly variable lengths (Supplementary Fig. 1c), progressively covering the microtubules (Fig. 1e and Supplementary Fig. 1d). During experimentally accessible time scales (approximately 1 h), island growth did not cease (Supplementary Fig. 1e). Notably, the tau density in the islands stayed constant during the period of growth (Fig. 1f and Supplementary Fig. 1f), suggesting that the islands grow by the addition of tau molecules at their boundaries, reminiscent of epitaxial growth of thin films. When the boundaries of neighbouring growing islands came into contact, the islands merged (Fig. 1c). At these instances, we never observed an increase in the tau density, suggesting that islands are formed by a well-defined tau layer occupying the entire accessible surface of the microtubule. When tau was removed from solution (Fig. 1g and Supplementary Video 2), tau molecules unbound rapidly and uniformly from all regions outside of islands (the 'island surroundings'), with a time constant of about 2 s, as inferred from the decay of the fluorescence signal (Fig. 1h, Supplementary Fig. 1g and Methods). By contrast, islands prevailed over several minutes, without substantial changes in the initial tau density, while slowly disassembling from their boundaries until they fully disappeared (Fig. 1g,h and Supplementary Fig. 1f). The island boundaries receded with an average velocity of approximately two tau molecules unbinding per second (Supplementary Fig. 1h and Methods). During disassembly, the islands occasionally underwent fission (Supplementary Fig. 1i). In contrast to the fast unbinding of tau from outside the islands, tau molecules unbound from the disassembling islands orders of magnitude slower—on the timescale of tens of minutes (Fig. 1h, Supplementary Fig. 1g and Methods). This extremely low unbinding rate explains the preservation of the islands in the absence of tau in solution and suggests that the occasional island fissions observed during disassembly occur after rare events of tau molecules unbinding from inside the island. Islands thus predominantly disassemble at their boundaries. The marked difference in the tau-unbinding rates inside and outside the islands, together with the assembly and disassembly kinetics at the island boundaries, strongly suggest that tau molecules in the islands cooperate, forming a cohesive layer on the microtubule surface. Because the N terminus of tau mediates tau–tau interactions[14], we repeated the experiments using a tau construct
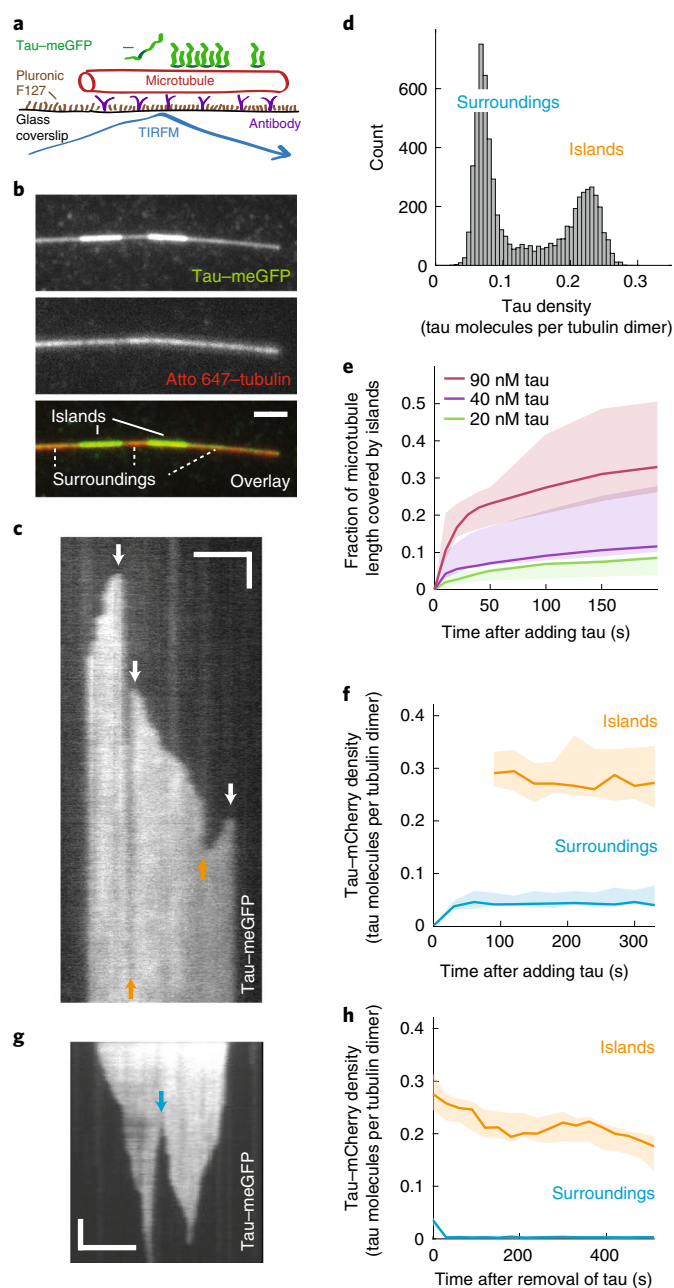
with a truncated N terminus (tau(ΔN)–meGFP; Supplementary Fig. 1j). Although tau(ΔN)–meGFP interacted with the microtubules, we did not observe any island formation even at tau(ΔN)–meGFP concentrations as high as 0.5 μM. Combined, these results show that full-length tau on microtubules can separate into two kinetically distinct phases, islands of high-density tau with slow turnover surrounded by regions of low-density tau with rapid turnover. Similar observations are reported in a complementary study by Tan et al.[15]

To investigate the dynamics of tau molecules in the islands, we incubated microtubules with 20 nM tau–mCherry and, after 15 min of incubation, replaced the assay buffer with a solution containing 20 nM tau–meGFP (Fig. 2a, Supplementary Fig. 2a and Supplementary Video 3). Tau–meGFP molecules exchanging with the leaving tau–mCherry, bound rapidly to the regions surrounding the islands, while binding with a slower time constant into the islands. In both islands and their surroundings, the turnover from tau–mCherry to tau–meGFP occurred without any positional preferences. Outside the islands, tau–mCherry rapidly dissociated from the microtubules with a time constant of about 3 s, comparable to the value estimated above when tau–meGFP was removed from solution (Supplementary Fig. 2b). Inside the islands, tau–mCherry dissociated with a time constant of about 20 s (Fig. 2b and Supplementary Fig. 2b), which, although an order of magnitude slower than outside the islands, was nevertheless substantially faster than the approximately 1,300 s measured in the absence of tau–meGFP in solution (Fig. 2b). At higher tau concentration (100 nM), we observed a further decrease in the time constant of tau–mCherry unbinding from the islands by about twofold, demonstrating that tau unbinding from the islands depends on the tau concentration in solution (Fig. 2b, Supplementary Fig. 2c and Methods). We did not observe such a trend in the low-density regions (Supplementary Fig. 2d).

To study the spatio-temporal dynamics of tau, we formed islands using a mixture of 20 nM tau–mCherry and 1 nM tau–meGFP, enabling us to observe the motion of individual tau–meGFP particles in an environment dominated by tau–mCherry (Fig. 2c). Fluorescence-intensity histograms of individual tau–meGFP particles has a single-Gaussian profile showing that tau–meGFP was incorporated in the islands as single molecules, highlighting that tau–tau interactions occurred only on the microtubule lattice (Supplementary Fig. 2e). Outside the islands, single tau–meGFP molecules diffused rapidly with a diffusion constant of $0.27 \pm 0.15\,\mu m^2 s^{-1}$ (linear fit coefficient $\pm$ 95% confidence bounds, Fig. 2c, Supplementary Fig. 2f and Methods), comparable to previously reported values[1]. By contrast, the tau–meGFP molecules in the islands were stationary, with a negligible diffusion constant of $0.027 \pm 0.016\,\mu m^2 s^{-1}$ (linear fit coefficient $\pm$ 95% confidence bounds, Fig. 2c and Supplementary Fig. 2f). Occasionally, single tau–meGFP molecules initially diffusing outside an island became stationary when associating with an island boundary (Fig. 2c). We conclude that the tau molecules localizing in the islands are sta-

Fig. 1 | Tau on microtubules separates into two kinetically distinct phases. **a**, Schematics depicting the assay geometry. **b**, Multichannel fluorescence micrograph showing islands of high-density tau–meGFP (bright green) surrounded by regions of low-density tau–meGFP (less intense green) on an Atto 647-labelled microtubule (red). Images taken 5 min after the addition of 20 nM tau–meGFP. **c**, Kymograph showing the fluorescence signal of tau–meGFP on a microtubule after the addition 20 nM tau–meGFP. Initially, the microtubule is covered by low tau–meGFP density. Over time, high-density tau–meGFP islands start to assemble. White arrows indicate positions of nucleation. Orange arrows indicate the merging of neighbouring islands growing towards each other. **d**, Distribution of fluorescence intensity of tau–meGFP along microtubules such as the one shown in **c**, showing two distinct populations. **e**, Fraction of microtubule length covered by tau islands after the addition of tau–meGFP (n = 3 experiments per condition, 131 microtubules). For statistics calculated over individual microtubules, see Supplementary Fig. 1d. **f**, Example time trace of the tau–mCherry density in the islands and their surroundings (Methods) after the addition of tau–mCherry (n = 5 microtubules). The tau–mCherry density within the islands was constant during the experiment. For quantification, see Supplementary Fig. 1f. **g**, Kymograph showing the fluorescence signal of tau–meGFP on the microtubule after the removal of tau–meGFP from solution, visualizing island disassembly. The blue arrow indicates a fission event. **h**, Example time trace of the tau–mCherry density inside and outside the islands after the removal of tau–mCherry from solution (n = 9 microtubules). Unbinding rates outside and inside the islands markedly differed and were in the order of seconds and tens of minutes, respectively (for quantification see Fig. 2b and Supplementary Figs. 1g and 2d). Experiments in **g** and **h** were performed with reduced framerate to minimize photobleaching (Methods). Experiments were repeated independently 438 (**b**), 343 (**c,d**), 22 (**f**), 115 (**g**) and 16 (**h**) times with similar results. In **e**, thick lines show the median and shaded areas indicate the full range of values; in **f** and **h**, thick lines show the median and shaded areas indicate the range between first and third quartiles. All scale bars, vertical 5 s, horizontal 2 μm.
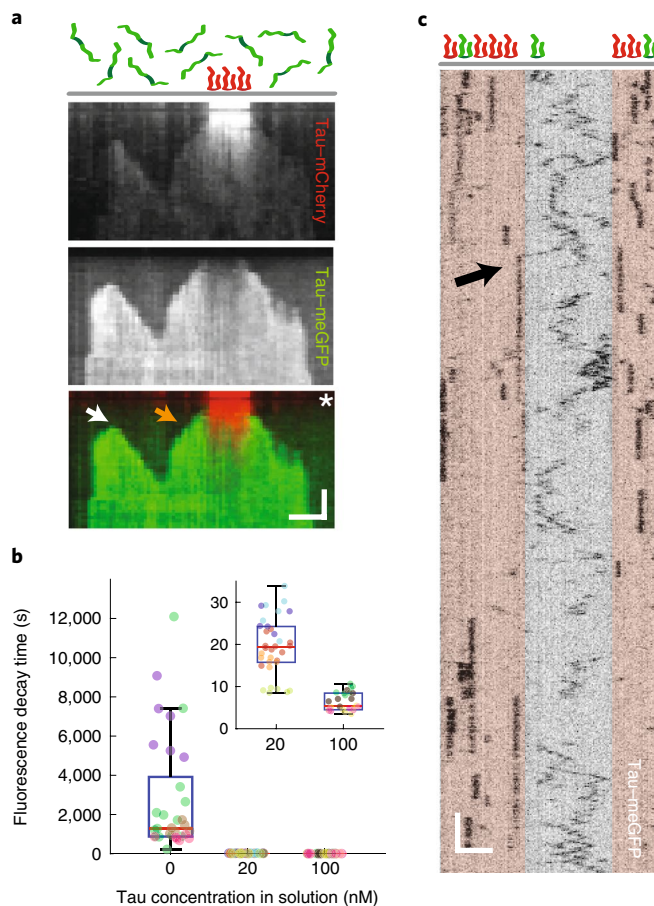
Fig. 2 | Tau molecules in the islands are stationary but exchange with tau in solution. a, Multichannel kymograph showing an island pre-formed in the presence of 20 nM tau–mCherry (red). After removing most of the tau–mCherry from solution by adding of 20 nM tau–meGFP (green; time of addition marked by white asterisk), we observed the exchange of tau–mCherry for tau–meGFP inside and outside of the islands. This exchange occurred along the entire length of the islands. Additionally, islands resumed their growth with the addition of tau–meGFP to their boundaries (an example is marked by an orange arrow). New islands also started to assemble (an example is marked by a white arrow). Scale bars: vertical 20 s, horizontal 2 μm. This experiment was repeated 15 times with similar results. **b**, The dwell time of fluorescently labelled tau in the islands decreases with increasing concentration of tau in solution (0 nM tau: dwell time 45 ± 46 min (mean ± s.d., n = 33 microtubules in 4 experiments; 20 nM tau: dwell time 20 ± 7 s (mean ± s.d., n = 34 microtubules in 5 experiments; 100 nM tau: dwell time 6.4 ± 2.1 s (mean ± s.d.), n = 26 microtubules in 4 experiments). The inset shows the 20 nM and 100 nM boxes on a magnified y scale. The data points are colour-coded by experiments. Typical time traces and corresponding fits underlying these data are shown in Supplementary Figs. 1g, 2b,c. For a description of all box-plot elements see Methods. **c**, Intensity-inverted kymograph showing single tau–meGFP molecules interacting with a microtubule containing two tau–mCherry islands (indicated by beige transparent boxes). Outside the islands, tau–meGFP diffuses rapidly, whereas inside the islands, tau–meGFP is stationary. Occasionally, we observed a diffusing tau–meGFP molecule stopping as it associated with an island (black arrow). Scale bars: vertical 1 s, horizontal 2 μm. This experiment was repeated 65 times with similar results.

tionary; nevertheless, as demonstrated above in bulk experiments (Fig. 2b) they can exchange with tau in solution.
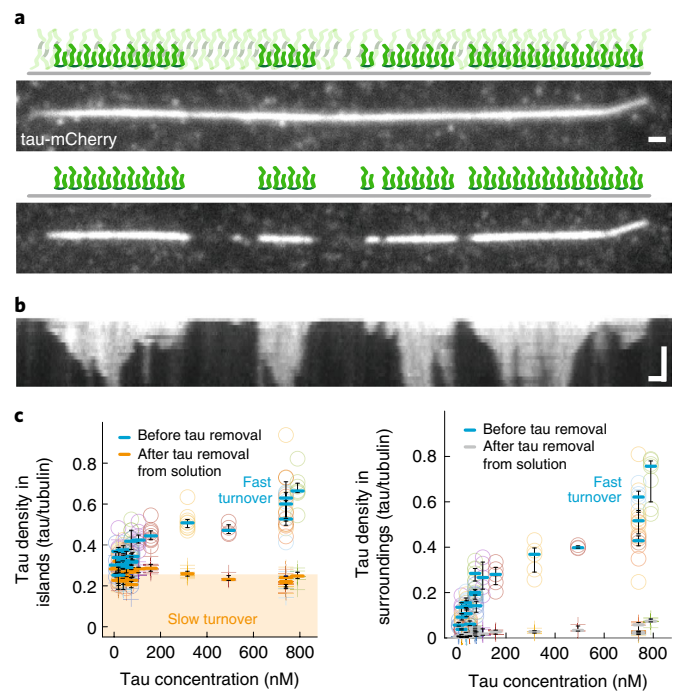
Fig. 3 | Tau islands are characterized by tau cohesion. a, Fluorescence micrographs showing the coverage of a microtubule by tau–mCherry. Top: uniform coverage at high (0.8 μM) concentration 5 min after the addition of tau–mCherry. Bottom: islands, 30 s after the removal of tau–mCherry from solution. This experiment was repeated 17 times with similar results. **b**, Kymograph of the experiment presented in **a**, showing the disassembly of the islands after the removal of tau–mCherry from solution. **c**, Tau densities in regions covered by islands and the surrounding regions established at various tau–meGFP concentrations, before and after the removal of tau–meGFP from solution (n = 150 microtubules, 21 experiments). Points are colour-coded by experiment, horizontal lines indicate the three quartiles of each experiment. The characteristic island density (main text, Methods) is indicated by the height of the shaded area (left panel). Scale bars: vertical 5 min, horizontal 1 μm.

To investigate the dependence of island formation on the concentration of tau, we performed experiments with repeated cycles of microtubule incubation with increasing concentrations of tau–meGFP followed by tau–meGFP removal from solution. Below a tau–meGFP concentration of approximately 5 nM, we did not observe any island formation (n = 245 microtubules in five experiments). Above this concentration, the tau–meGFP density outside and inside the islands increased with increasing tau–meGFP concentration in solution. After each removal of tau–meGFP, the tau density in the regions surrounding the islands returned to the background level within several seconds (Supplementary Fig. 3a; consistent with the data shown in Fig. 1h). By contrast, after each removal of tau–meGFP, the tau density in the islands decayed in two stages: within a few seconds, a fast density drop occurred uniformly along the whole length of the islands, followed by a slow density decrease, the latter consistent with the data shown in Fig. 1h (Supplementary Fig. 3a). Above a tau–meGFP concentration of approximately 0.5 μM, the tau density on the microtubules reached saturation (Supplementary Fig. 3b), as previously reported[16], suggesting that tau associates with a finite number of interaction sites on the microtubule. In this regime, the islands became apparent only after tau–meGFP was removed from solution, following which tau–meGFP rapidly unbound from the surroundings and islands became discernable (Fig. 3a,b). Of note, in all experiments, the tau–meGFP

density in the islands, after the fast density drop, had the same value of 0.26 ± 0.05 tau molecules per tubulin dimer (mean $\pm$ s.d., $n = 101$ microtubules, 14 experiments; Methods), independent of the initial tau concentration in solution (Fig. 3c). Together with the results in Figs. 1 and 2, these experiments show that cohesive islands on microtubules are formed by tau molecules that bind cooperatively and, consequently, turn over slowly. At physiological tau concentrations[17] in the range of 0.5–1.5 µM, tau molecules, which turn over rapidly, co-localize with islands. These tau molecules, whose density depends on the tau concentration in solution in a similar way as the tau density outside the islands (Supplementary Fig. 3c), do not appear to participate in the cooperative island formation.

To investigate how the tau islands may regulate the interaction of other MAPs with microtubules, we formed tau islands using tau–mCherry and tested their effect on GFP-tagged MAPs. First, we tested the molecular motor kinesin-1. After addition of 60 nM kinesin-1–GFP (Methods) to microtubules in the presence of tau–mCherry, we observed processive movement of single motors outside the islands (Fig. 4a and Supplementary Fig. 4a,b). On reaching the island boundaries, the motors dissociated instantaneously from the microtubules (Fig. 4a), similar to previous observations of kinesin-1 encountering static obstacles[18,19]. The kinesin-1 landing rate in the islands was about an order of magnitude lower than in their surroundings (Supplementary Fig. 4c). Notably, at all studied tau concentrations, no kinesin-1 molecules landing inside an island moved processively (total number of 553 molecules in 23 experiments); instead, these transient interactions were static. Second, we tested the microtubule-severing enzyme katanin. After the addition of 200 nM katanin–GFP (subunits p60 and p80[20]) to microtubules in the presence of 20 nM tau–mCherry, we observed katanin–GFP binding and microtubule severing predominantly outside the islands, leading to the disintegration of these microtubule regions (Fig. 4b, Supplementary Fig. 4d and Supplementary Video 4), while island-covered regions prevailed. On longer time scales, the island-covered regions of the microtubules started to disassemble slowly

from their boundaries, with only occasional isolated cut observed in the island-covered microtubules (Fig. 4b, Supplementary Fig. 4e and Supplementary Video 4). Whereas non-island microtubule regions disassembled within 1 min, the island-protected microtubule stretches persisted on the timescale of tens of minutes. Third, we tested the effect of the tau islands on superprocessive motors. We used *Saccharomyces cerevisiae* Kip3, the best described member of the kinesin-8 family. Unlike kinesin-1[18,19], Kip3 does not dissociate from the microtubule when the next binding site ahead is occupied, but rather pauses for extended periods of time[21], leading to the formation of 'traffic jams'[22]. As the kinesin- and tau- interaction sites on microtubules overlap[23], we hypothesized that traffic jams might form in front of tau islands. We formed islands using 20 nM or 100 nM tau–mCherry. After the addition of 15 nM Kip3–GFP, we observed Kip3–GFP molecules moving in the low-density tau regions. In contrast to kinesin-1, we also detected Kip3–GFP motility inside the tau islands, albeit at decreased velocity and

Fig. 4 | Tau islands constitute a protective layer around microtubules.
a, Fluorescence kymograph showing kinesin-1–GFP molecules moving processively outside the islands and immediately dissociating from the microtubule when reaching the island boundaries (island positions indicated by schematics above the kymograph). No kinesin-1–GFP molecules moved processively inside the islands. This experiment was repeated 124 times with similar results. For quantification of the kinesin-1–GFP landing rates inside and outside the islands, and velocities and dwell times outside the islands at different tau concentrations, see Supplementary Fig. 4a–c. **b**, Multichannel fluorescence micrographs showing katanin–GFP-driven (green, example position indicated by green arrow) severing of Atto 647 microtubules (blue) decorated with tau–mCherry islands (red, example indicated by red arrow) interspersed by regions of low tau–meGFP density (indicated by blue arrow). Katanin–GFP was added at time = 0 s. Initially, microtubule severing and disassembly occurred only in the regions surrounding the islands (example indicated by white arrow). On longer time scales katanin–GFP induced shortening of the island-covered regions of the microtubule (example indicated by yellow arrow). This experiment was repeated 11 times with similar results. **c**, Multichannel fluorescence micrographs showing that Kip3–GFP (kinesin-8, green) localizes both outside and inside the tau–mCherry (red) islands (exemplary localization of Kip3–GFP in the island indicated by green arrow) on Atto 647-labelled microtubules (blue) and accumulates at the microtubule ends (yellow arrow) and in front of the islands (white arrow). This experiment was repeated seven times with similar results. **d**, Multichannel fluorescence micrographs showing that Kip3–GFP (green) accumulating in front of a tau–mCherry island (red) can remove the island by displacing tau–mCherry from the island edge (receding of the island boundary indicated by white arrow). Scale bars: vertical 1 s, horizontal 2 µm.
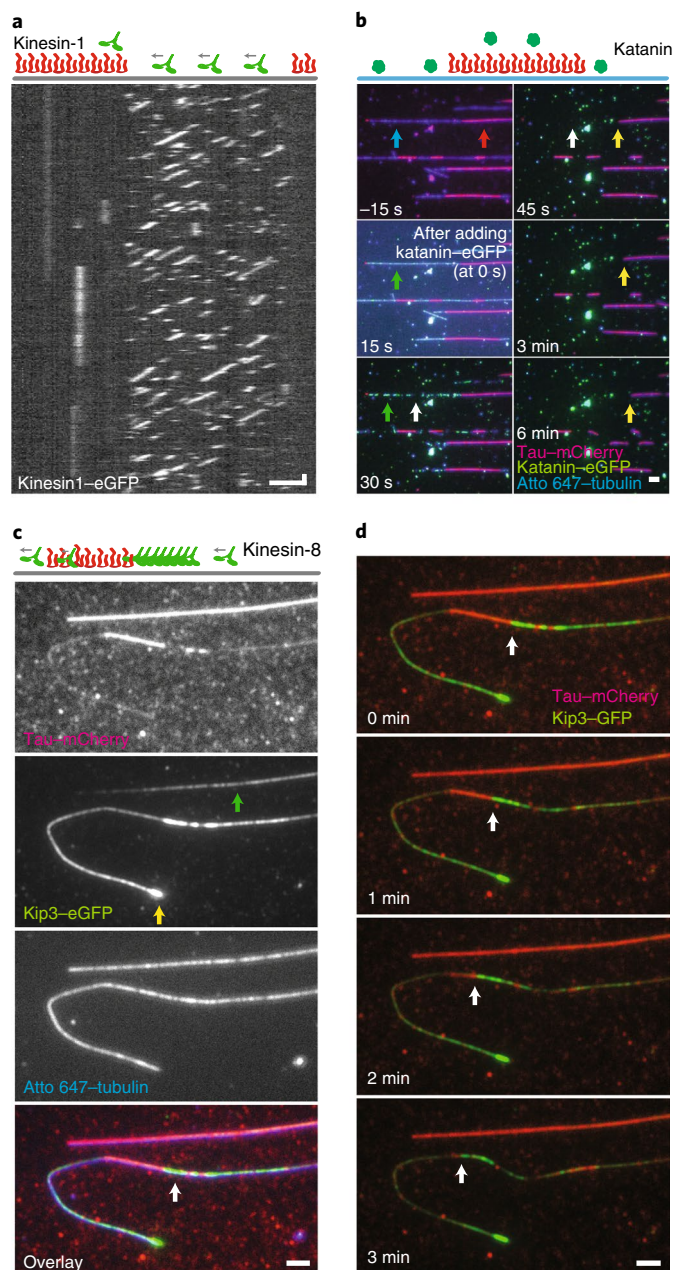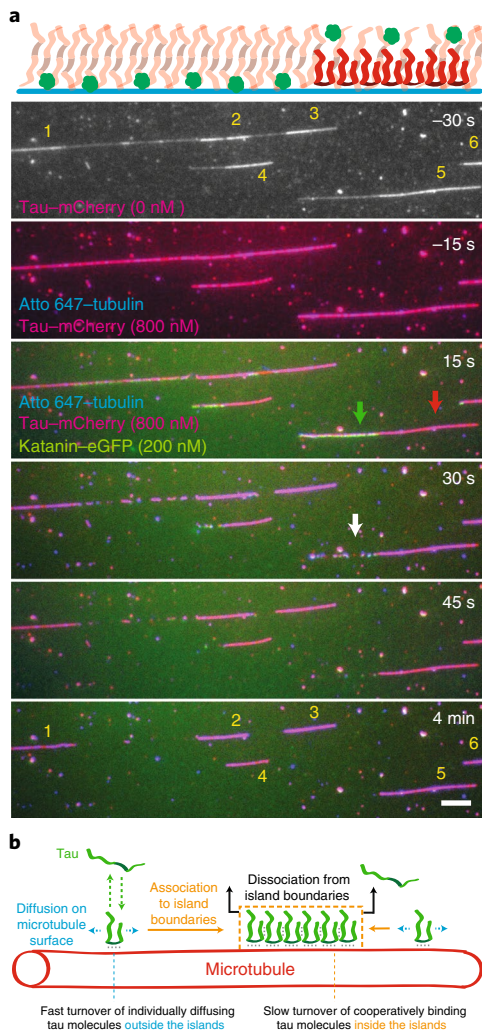
Fig. 5 | Microtubule shielding depends on tau cohesion in the islands.
a, Multichannel fluorescence micrographs showing katanin–GFP-driven (green) severing of Atto 647-microtubules (blue) decorated with tau–mCherry islands (red) formed at 0.8 μM tau–mCherry. The island positions (indicated by numbers) were determined after a brief removal of tau–mCherry from solution (time = −30 s, Methods). After 0.8 μM tau–mCherry was re-introduced, microtubules became uniformly covered by tau–mCherry (time = −15 s). Katanin–GFP was added at time = 0 s. Katanin–GFP was recruited to regions outside the islands (example indicated by green arrow) and excluded from the islands (example indicated by red arrow). Microtubule severing and disassembly occurred initially only in the regions outside the islands (example indicated by white arrow). Over longer time scales, islands disassembled from their boundaries (compare to Fig. 4b). Scale bar, 2 μm. This experiment was repeated 11 times with similar results. **b**, Schematic representation of island formation. Tau molecules bind and unbind with high rates to microtubules, on which they diffuse (fast turnover). When encountering an island (dashed orange box), tau molecules cooperatively associate with the island at its boundaries, rendering the tau molecules stationary, decreasing their unbinding rate (slow turnover), and causing the island to grow in size laterally. Tau molecules from solution can only bind to the inside of an island via displacement of an island-associated tau molecule, resulting in the observed concentration-dependent turnover of tau inside islands. After removal of tau from solution, tau molecules dissociate from the island boundaries, making the island shrink in size laterally.

density (Fig. 4c,d, Supplementary Fig. 4f–h and Supplementary Video 5). Notably, we observed that Kip3–GFP moving in the low-density tau regions accumulated at the boundaries of the tau

islands (Fig. 4c). The resulting high-density traffic jams caused enhanced unbinding of tau–mCherry at these positions, eventually leading to the displacement of the islands (Fig. 4d) at velocities comparable to Kip3–GFP walking within islands (Supplementary Fig. 4g and Supplementary Fig. 4i). These combined results show that tau islands constitute a protective layer on the microtubule surface, which blocks kinesin-1-based transport and obstructs the severing activity of katanin, and that the activity of superprocessive motors can displace existing islands from the microtubule surface.

Because the island and non-island regions exhibited similar tau densities under saturating, physiological tau concentrations (Fig. 3), we considered whether, under these conditions, the diffusible tau molecules in the non-island regions could shield the microtubules against severing. We therefore: (1) formed islands using 0.8 μM tau–mCherry, (2) after 5 min, briefly removed tau–mCherry from solution to note the position of the islands, and (3) re-introduced 0.8 μM tau–mCherry. We then immediately exposed these tau–mCherry fully decorated microtubules to 200 nM katanin–GFP analogously to the experiment presented in Fig. 4b. We observed, similarly to Fig. 4b, that the non-island regions were severed and rapidly disassembled, whereas the island-covered microtubules persisted and only slowly disassembled from their boundaries with an occasional cut in the islands (Fig. 5a, Supplementary Fig. 4d,e and Supplementary Video 6). These experiments show that the density of tau does not determine whether tau forms a protective layer around microtubules. Rather, the microtubule protection is enabled by the cohesion between the cooperatively binding tau molecules that make up the islands (Fig. 5b).

Tau islands displayed a characteristic density of about 0.26 tau molecules per tubulin dimer, suggesting that tau molecules bind to the microtubule in an ordered monolayer, presumably engaging all four microtubule-binding repeats, whose positions at a similar density were shown recently using cryo-electron microscopy[23]. At physiological tau levels (0.5 μM and above), rapidly turning-over tau co-localized with the islands. The transience of these interactions explains why this pool of tau could not be captured by cryo-electron microscopy. Our results suggest that the integrity of the islands depends on cooperativity between the constituent tau molecules. Consistent with this notion, tau molecules on microtubules interact with each other[9,24], in solution can undergo liquid–liquid phase separation[25] or, when hyperphosphorylated, form neurofibrillary tangles[6]. It seems plausible that tau–tau interactions, in addition to the binding of the four tau repeats to the microtubule, underpin the formation of islands. Alternatively, or in addition, cooperativity could depend on the number of microtubule protofilaments, as observed for doublecortin[26], and/or on a local tau-induced modification of the microtubule surface translating along the microtubule lattice into adjacent binding sites and locally increasing the affinity for incoming tau molecules.

Tau unbinding from the islands increases with increasing tau concentration in solution. This observation cannot be attributed to the pool of rapidly turning-over tau, which colocalizes with the island-incorporated tau at high concentrations (Fig. 3). At the concentrations tested (20 nM and 100 nM), this pool accounts for only approximately 20% and 40% of the total number of tau in the islands (Fig. 3c), respectively, whereas the average unbinding time decreases by two orders of magnitude. We interpret this phenomenon as the consequence of a multivalent attachment of island-incorporated tau mediated by the four microtubule-binding repeats of tau and tau–tau interaction sites. These bonds individually undergo transient cycles of unbinding and rebinding. At low tau concentration, transiently released bonds are probably re-established, as a partially bound tau molecule remains anchored to the microtubule via its persisting binding sites, keeping the released binding interfaces in close proximity. With increasing tau concentration in solution however, it becomes increasingly probable that a binding site

of a tau molecule from solution establishes a bond to a temporarily-vacated binding site on the microtubule and thereby, might replace an island-incorporated tau molecule, one bond at a time. Unbinding rates that depend on the concentration of ligands in solution, as previously reported for other multivalently interacting macromolecules[27,28], may also explain the kinesin-8-driven island disassembly. Kinesin-8 does not dissociate when an adjacent binding site on the microtubule is occupied. Instead, the motor pauses in front of a bound tau molecule until, stochastically, this next binding site becomes available by transient unbinding of a microtubule-binding repeat of tau. Kinesin-8 is then favourably positioned to occupy this site on the microtubule and thereby sequentially replace all the microtubule-binding repeats of a tau molecule. In this way, super-processive motors might regulate the localization of tau in neurons. Reciprocally, these motors might be regulated by tau islands, by the formation of traffic jams at their boundaries and reduction of their speed in the island-covered regions.

Highly curved microtubule regions show increased tau binding[29], similar to that of doublecortin[30]. Indeed we observed that tau in regions of highly curved microtubules (radius < 2.5 μm) exhibited higher density than in surrounding regions, but lower than in the islands on straight microtubule regions (Supplementary Fig. 5a (top),b, c). Of note, the highly curved regions were not protected from katanin-mediated severing (Supplementary Fig. 5a,d, Supplementary Video 7), demonstrating that tau molecules in the highly curved regions do not form a cohesive layer. Also, tau–meGFP binding in the curved regions was distinct from island formation on straight microtubules (Supplementary Fig. 5e–h). These results suggest suggest that high microtubule curvatures, though attracting tau, prevent the formation of cohesive tau islands.

In summary, we show that tau on microtubules can coexist in two kinetically distinct phases, resulting in the formation of cohesive tau islands. Complementary work by Tan et al. confirms the existence of these cohesive regions and demonstrate their significance for the regulation of cytoplasmic dynein and spastin[15]. We hypothesize that islands may act as a readout of post-translational tubulin modifications, rendering these regions differentially accessible to other MAPs. Furthermore, other intrinsically disordered proteins, analogously, might also be able to form cohesive islands on microtubules, which could add a further layer of MAP sorting and regulation on microtubules, as suggested recently[31]. It is an intriguing possibility that in neurodegenerative diseases, diminished island assembly—triggered, for example, by hyperphosphorylation of tau—could cause various downstream pathophysiological effects.

Online content

Any methods, additional references, Nature Research reporting summaries, source data, statements of code and data availability and associated accession codes are available at https://doi.org/10.1038/s41556-019-0374-6.

References

1. Hinrichs, M. H. et al. Tau protein diffuses along the microtubule lattice. *J. Biol. Chem.* **287**, 38559–38568 (2012).
2. Kneynsberg, A., Combs, B., Christensen, K., Morfini, G. & Kanaan, N. M. Axonal degeneration in tauopathies: disease relevance and underlying mechanisms. *Front. Neurosci.* **11**, 572 (2017).
3. Qiang, L. Tau protects microtubules in the axon from severing by katanin. *J. Neurosci.* **26**, 3120–3129 (2006).
4. Morris, M., Maeda, S., Vossel, K. & Mucke, L. The many faces of tau. *Neuron* **70**, 410–426 (2011).
5. Gao, Y.-L. et al. Tau in neurodegenerative disease. *Ann. Transl. Med.* **6**, 175–175 (2018).
6. Iqbal, K., Liu, F. & Gong, C.-X. Tau and neurodegenerative disease: the story so far. *Nat. Rev. Neurol.* **12**, 15–27 (2016).
7. Drechsel, D. N., Hyman, A. A., Cobb, M. H. & Kirschner, M. W. Modulation of the dynamic instability of tubulin assembly by the microtubule-associated protein tau. *Mol. Biol. Cell* **3**, 1141–1154 (1992).
8. Chaudhary, A. R., Berger, F., Berger, C. L. & Hendricks, A. G. Tau directs intracellular trafficking by regulating the forces exerted by kinesin and dynein teams. *Traffic* **19**, 111–121 (2018).
9. Dixit, R., Ross, J. L., Goldman, Y. E. & Holzbaur, E. L. F. Differential regulation of dynein and kinesin motor proteins by Tau. *Science* **319**, 1086–1089 (2008).
10. Vershinin, M., Carter, B. C., Razafsky, D. S., King, S. J. & Gross, S. P. Multiple-motor based transport and its regulation by Tau. *Proc. Natl Acad. Sci. USA* **104**, 87–92 (2007).
11. Seitz, A. et al. Single-molecule investigation of the interference between kinesin, tau and MAP2c. *EMBO J.* **21**, 4896–4905 (2002).
12. Trinczek, B., Ebneth, A., Mandelkow, E. M. & Mandelkow, E. Tau regulates the attachment/detachment but not the speed of motors in microtubule-dependent transport of single vesicles and organelles. *J. Cell Sci.* **112**, 2355–2367 (1999).
13. Ebneth, A. et al. Overexpression of tau protein inhibits kinesin-dependent trafficking of vesicles, mitochondria, and endoplasmic reticulum: implications for Alzheimer's disease. *J. Cell Biol.* **143**, 777–794 (1998).
14. Gamblin, T. C., Berry, R. W. & Binder, L. I. Tau polymerization: role of the amino terminus. *Biochemistry* **42**, 2252–2257 (2003).
15. Tan, R. et al. Microtubules gate tau condensation to spatially regulate microtubule functions. *Nat. Cell Biol.* https://doi.org/10.1038/s41556-019-0375-5 (2019).
16. Makrides, V., Massie, M. R., Feinstein, S. C. & Lew, J. Evidence for two distinct binding sites for tau on microtubules. *Proc. Natl Acad. Sci. USA* **101**, 6746–6751 (2004).
17. Wegmann, S. et al. Tau protein liquid–liquid phase separation can initiate tau aggregation. *EMBO J.* **37**, e98049 (2018).
18. Schneider, R., Korten, T., Walter, W. J. & Diez, S. Kinesin-1 motors can circumvent permanent roadblocks by side-shifting to neighboring protofilaments. *Biophys. J.* **108**, 2249–2257 (2015).
19. Telley, I. A., Bieling, P. & Surrey, T. Obstacles on the microtubule reduce the processivity of Kinesin-1 in a minimal in vitro system and in cell extract. *Biophys. J.* **96**, 3341–3353 (2009).
20. Jiang, K. et al. Microtubule minus-end regulation at spindle poles by an ASPM–katanin complex. *Nat. Cell Biol.* **19**, 480–492 (2017).
21. Varga, V., Leduc, C., Bormuth, V., Diez, S. & Howard, J. Kinesin-8 motors act cooperatively to mediate length-dependent microtubule depolymerization. *Cell* **138**, 1174–1183 (2009).
22. Leduc, C. et al. Molecular crowding creates traffic jams of kinesin motors on microtubules. *Proc. Natl Acad. Sci. USA* **109**, 6100–6105 (2012).
23. Kellogg, E. H. et al. Near-atomic model of microtubule–tau interactions. *Science* **360**, 1242–1246 (2018).
24. McVicker, D. P., Hoeprich, G. J., Thompson, A. R. & Berger, C. L. Tau interconverts between diffusive and stable populations on the microtubule surface in an isoform and lattice specific manner. *Cytoskeleton* **71**, 184–194 (2014).
25. Hernández-Vega, A. et al. Local nucleation of microtubule bundles through tubulin concentration into a condensed Tau phase. *Cell Rep.* **20**, 2304–2312 (2017).
26. Bechstedt, S. & Brouhard, G. J. Doublecortin recognizes the 13-protofilament microtubule cooperatively and tracks microtubule ends. *Dev. Cell* **23**, 181–192 (2012).
27. Sing, C. E., Olvera de la Cruz, M. & Marko, J. F. Multiple-binding-site mechanism explains concentration-dependent unbinding rates of DNA-binding proteins. *Nucleic Acids Res.* **42**, 3783–3791 (2014).
28. Lansky, Z. et al. Diffusible crosslinkers generate directed forces in microtubule networks. *Cell* **160**, 1159–1168 (2015).
29. Samsonov, A., Yu, J.-Z., Rasenick, M. & Popov, S. V. Tau interaction with microtubules in vivo. *J. Cell Sci.* **117**, 6129–6141 (2004).
30. Bechstedt, S., Lu, K. & Brouhard, G. J. Doublecortin recognizes the longitudinal curvature of the microtubule end and lattice. *Curr. Biol.* **24**, 2366–2375 (2014).
31. Monroy, B. Y. et al. Competition between microtubule-associated proteins directs motor transport. *Nat. Commun.* **9**, 1714 (2018).

Acknowledgements

Author contributions

Competing interests

The authors declare no competing interests.

Additional information

Supplementary information is available for this paper at https://doi.org/10.1038/s41556-019-0374-6.

Reprints and permissions information is available at www.nature.com/reprints.

Correspondence and requests for materials should be addressed to A.H.-V., Z.L. or M.B.

Publisher's note: Springer Nature remains neutral with regard to jurisdictional claims in published maps and institutional affiliations.

Methods

Protein purification. meGFP- or mCherry-tagged tau and tau(ΔN), kinesin-1, Kip3 and katanin were expressed and purified as described previously[20,25,32,33].

In vitro tau–microtubule binding assay. Microtubules and flow chambers were prepared as described previously[33,34]. Biotinylated, paclitaxel-stabilized, Atto 647-labelled microtubules in BRB80T (80 mM PIPES–KOH pH 6.9, 1 mM MgCl$_2$, 1 mM EGTA and 10 μM paclitaxel) were immobilized in a flow chamber using biotin antibody (Sigma B3640, 20 μg ml^{-1} in PBS). Subsequently, the buffer in the flow chamber was exchanged for assay buffer (20 mM HEPES pH 7.4, 1 mM EGTA, 75 mM KCl, 2 mM MgCl$_2$, 1 mM Mg-ATP, 10 mM dithiothreitol, 0.02 mg ml^{-1} casein, 10 μM paclitaxel, 20 mM D-glucose, 0.22 mg ml^{-1} glucose oxidase and 20 μg ml^{-1} catalase). Tau in assay buffer was then flushed into the flow chamber at the final assay concentration as indicated in the text. To test the robustness of island assembly, we observed island assembly under different conditions of ionic strength (0–125 mM KCl additional to the assay buffer), pH (6.8–7.4) and buffering agent (20 mM HEPES, 50 mM HEPES and 80 mM PIPES). In experiments including multiple subsequent tau additions, the flow chamber was rinsed between each tau addition with high ionic strength buffer (125 mM KCl additional to the assay buffer). To remove tau from solution, the chamber was perfused with approximately four times the chamber volume using assay buffer without tau. For high concentrations of tau (>200 nM), higher volumes (up to ten times the chamber volume) were used to remove tau. In experiments involving kinesin-8, katanin or kinesin-1, islands were first pre-formed before the respective protein was added to the solution (keeping the tau concentration constant). For the katanin experiment at elevated tau concentration (Fig. 5), microtubules were first incubated with 0.8 μM tau–mCherry for 5 min. Tau–mCherry was then briefly removed from the measurement chamber (less than 1 min) for the positions of the islands to be recorded (they were obscured by the high tau–mCherry density in the island surroundings). Tau–mCherry was then added at 0.8 μM. Subsequently, 200 nM katanin–GFP was added to the solution (while maintaining the tau concentration at 0.8 μM). All experiments were performed at room temperature.

Imaging. Atto 647-labelled microtubules and mCherry- and meGFP-labelled proteins were visualized sequentially by switching between the Cy5, TRITC and GFP channels (Chroma filter cubes) on a Nikon-Ti E microscope equipped with a ×100 Nikon TIRFM objective and either Hamamatsu Orca Flash 4.0 sCMOS or Andor iXon EMCCD cameras. The acquisition rate varied between 1 frame per 30 ms to 1 frame per 10 min, depending on the experiment and is indicated in the corresponding figure. Imaging conditions in experiments used for quantitative estimation of kinetic parameters were set such that photobleaching effects were negligible (<2% fluorescent intensity loss during the experiment). Experiments were performed over several months by three researchers. Each experiment was repeated at least on three days. No data was excluded from the study.

Image analysis. Data was analysed using FIJI v.1.52[35] and custom Matlab (Mathworks) routines.

Tau density estimation. Kymographs (using FIJI KymographBuilder plugin, modified to compute integrated intensity instead of finding the maximum intensity) along the microtubule length were used to read out the meGFP or mCherry fluorescent signal and to estimate the integrated signal intensity of meGFP- or mCherry-labelled tau bound to the microtubule (if necessary, time series were drift-corrected with the FIJI plugin 'image stabilizer'). The meGFP signal in regions directly adjacent to the microtubule was estimated in the same way, smoothed with a moving median along the microtubule length and subtracted as background signal. The kymograph pixels were then manually categorized according to the type of microtubule region they covered (islands, regions surrounding the islands, or regions of highly curved microtubules with an increased tau density). The integrated intensity of tau for a region on a microtubule was then computed for each frame by taking the sum of the categorized kymograph pixels. The density of meGFP- or mCherry-labelled tau bound to the microtubule was then estimated by dividing the integrated intensity by the estimated intensity per single fluorescent molecule (either mCherry or meGFP, see below) and the length of the region. Conversion to the number of tau molecules per tubulin dimer was performed assuming tau binding to 13 protofilaments and an 8 nm length of tubulin dimer. The Kip3 densities were estimated analogously: tau–mCherry islands were identified in the corresponding channel (561 nm), and density traces of Kip3–GFP (488 nm) were read out at the corresponding locations.

Single fluorophore quantification. Fluorescent signal of a single fluorescent molecule (meGFP or mCherry) was determined by generating intensity time traces of single meGFP- or mCherry-labelled kinesin-1 molecules tightly bound to the microtubule in presence of adenylyl-imidodiphosphate (in the absence of ATP) and estimating the 'height' of the bleaching steps. The number of steps was first estimated by eye, and this number was used as input for the findchangepoints function of Matlab to determine the position of the steps (by detection of significant changes of the mean value). To yield the intensity per single molecule,

the median of the heights of these steps was calculated. The number of averaged steps was at least 15 per estimate. Photobleaching rates (at the given imaging conditions, on the day of the experiment) were determined using the experimental setup described above. Instead of single-molecule intensities, the integrated intensity of all labelled kinesin-1 molecules was measured.

The fraction of microtubule length covered by tau islands. The fraction of microtubule length covered by tau islands was estimated by approximating islands and microtubules with segmented lines, measuring their lengths and dividing the sum of the lengths of the islands on a single microtubule (or in a field of view) by the length of the respective microtubule on which the islands are located (or by the summed length of all microtubules in a field of view).

Estimation of the tau-unbinding time. To estimate the unbinding times of tau inside and outside the islands, we analysed how the tau density in a given region decayed over time after a buffer exchange that either removed tau from solution or replaced tau–meGFP in the solution with tau–mCherry. Every analysed region (island or surrounding) yielded a time trace of tau density decay after a buffer exchange. Time traces from exemplary experiments were combined to be presented in Fig. 1f,h, Supplementary Figs. 1g, 2b,c; the line represents the median value of all traces at the given point in time and the edges of the shaded area represent the first and third quartiles. To estimate the mean residence times of tau inside and outside the islands, individual density time traces as described above were fitted separately by an exponential decay using the Matlab function 'fit' (data points taken before exchange of solution were not taken into account). The presented fits and mean residence times were computed by averaging the coefficients of the individual fits.

Estimation of velocity and diffusion coefficient. Tracking of single tau molecules for the estimation of diffusion coefficient was performed using FIESTA[36] software. To reconnect tracks, a threshold velocity of 12,000 nm s^{-1} was chosen, and tracks were allowed to have at most three missing frames between two data points. To minimize false-positive connections of molecules, the tracks obtained by FIESTA were cut such that the maximum distance between two data points was never more than 360 nm. Island boundary assembly and disassembly velocities (in the absence or presence of katanin or Kip3) were estimated by approximating straight lines onto segments of advancing or receding tau-island edges in kymographs. The value presented in the text is a duration-weighted average of the corresponding segments. This was converted to the number of tau molecules per second by multiplying this velocity by the estimated characteristic tau density within islands (in molecules per nanometre), assuming tau binding to 13 protofilaments and 8 nm length per tubulin dimer. Kip3 and kinesin-1 velocities were estimated by approximating straight lines onto kymographs of moving motors (inside and outside islands).

Katanin severing-rate estimation. Severing rates in the areas surrounding the islands were estimated by fitting exponential decay to the number of pixels in the area of the original microtubule position above a threshold value, which was manually set to encompass the microtubule. In island regions, cuts were counted. In Supplementary Fig. 4e, the estimated severing rates include both straight and curved microtubules. In Supplementary Fig. 5d, the severing rates are sorted according to the following definition: straight microtubules were defined as microtubule stretches in which the microtubule orientation would not change beyond 10°; curved regions were defined as 0.5 μm-long stretches of microtubule centred at the point of highest curvature with radius <2.5 μm.

Data representation. In all box plots presented in the figures, the horizontal midline indicates the median; bottom and top box edges indicate the 25th and 75th percentiles, respectively; the whiskers extend to the most extreme data points not considered as outliers (the function 'Alternative box plot' from the IoSR Matlab Toolbox has been used). Thick lines with shaded areas, unless otherwise indicated, show the median and the 25th and 75th percentiles. Where single data points are presented, points from the same experiment are indicated by the same colour (unless otherwise stated). The individual data points have been weighted such that each experiment carries the same weight for determination of the median and percentile lines. Weighting by experiments has been performed in all data represented in the text or in figures involving averages or quartiles, except for the determination of the diffusion constants of tau, where each experiment was weighted according to how many tau molecules were observed in the respective experiment.

Statistics and reproducibility. Experiments were performed over several months by three researchers; all replication attempts (that were not impeded by unrelated events, such as an image-acquisition-software malfunction) were successful. For each quantified experiment and each exemplary image or kymograph, N describes the number of either biologically independent samples (individual tau molecules, islands of tau molecules or microtubules) or the number of independent events (island nucleation, island merging or island fission). In all cases, the number of independent experiments, during which the data were gathered over the course

of several days, refers to the number of independent flow channels, which were assembled, filled with assay components and imaged individually.

Reporting Summary. Further information on research design is available in the Nature Research Reporting Summary linked to this article.

Data availability

Source data for Figs. 1–5 and quantifications given in the main text (island density) have been provided as Supplementary Table 1. Example raw videos are available at BioStudies with accession number S-BSST266. All other data supporting the findings of this study are available from the corresponding authors on reasonable request.

Code availability

Code used to determine single-molecule intensities (GNU General Public License v.3, for further information see repository) is available at https://doi.org/10.5281/ zenodo.3270568. Code used to create kymographs (MIT license, for further information see repository) is available at https://doi.org/10.5281/zenodo.3270572. All other custom written code is available from the corresponding authors on request.

References

32. Mitra, A., Ruhnow, F., Girardo, S. & Diez, S. Directionally biased sidestepping of Kip3/kinesin-8 is regulated by ATP waiting time and motor-microtubule interaction strength. *Proc. Natl Acad. Sci. USA* **115**, E7950–E7959 (2018).
33. Nitzsche, B. et al. Studying kinesin motors by optical 3D-nanometry in gliding motility assays. *Methods Cell Biol.* **95**, 247–271 (2010).
34. Braun, M. et al. Adaptive braking by Ase1 prevents overlapping microtubules from sliding completely apart. *Nat. Cell Biol.* **13**, 1259–1264 (2011).
35. Schindelin, J. et al. Fiji: an open-source platform for biological-image analysis. *Nat. Methods* **9**, 676–682 (2012).
36. Ruhnow, F., Zwicker, D. & Diez, S. Tracking single particles and elongated filaments with nanometer precision. *Biophys. J.* **100**, 2820–2828 (2011).

naturereseachR

Corresponding author(s): Stefan Diez
Zdenek Lansky
Marcus Braun

Last updated by author(s): Jul 9, 2019

Reporting Summary

Nature Research wishes to improve the reproducibility of the work that we publish. This form provides structure for consistency and transparency in reporting. For further information on Nature Research policies, see Authors & Referees and the Editorial Policy Checklist.

Statistics

For all statistical analyses, confirm that the following items are present in the figure legend, table legend, main text, or Methods section.

n/a	Confirmed	
☐	☒	The exact sample size (*n*) for each experimental group/condition, given as a discrete number and unit of measurement
☐	☒	A statement on whether measurements were taken from distinct samples or whether the same sample was measured repeatedly
☒	☐	The statistical test(s) used AND whether they are one- or two-sided *Only common tests should be described solely by name; describe more complex techniques in the Methods section.*
☒	☐	A description of all covariates tested
☒	☐	A description of any assumptions or corrections, such as tests of normality and adjustment for multiple comparisons
☐	☒	A full description of the statistical parameters including central tendency (e.g. means) or other basic estimates (e.g. regression coefficient) AND variation (e.g. standard deviation) or associated estimates of uncertainty (e.g. confidence intervals)
☒	☐	For null hypothesis testing, the test statistic (e.g. *F*, *t*, *r*) with confidence intervals, effect sizes, degrees of freedom and *P* value noted *Give P values as exact values whenever suitable.*
☒	☐	For Bayesian analysis, information on the choice of priors and Markov chain Monte Carlo settings
☒	☐	For hierarchical and complex designs, identification of the appropriate level for tests and full reporting of outcomes
☒	☐	Estimates of effect sizes (e.g. Cohen's *d*, Pearson's *r*), indicating how they were calculated

Our web collection on statistics for biologists contains articles on many of the points above.

Software and code

Policy information about availability of computer code

Data collection	Microscopy data were collected using Nikon NIS Elements 5.0.2.
Data analysis	Data were analyzed using FIJI 2.0.0, Matlab 2016 and Fiesta 1.05.

For manuscripts utilizing custom algorithms or software that are central to the research but not yet described in published literature, software must be made available to editors/reviewers. We strongly encourage code deposition in a community repository (e.g. GitHub). See the Nature Research guidelines for submitting code & software for further information.

Data

Policy information about availability of data

All manuscripts must include a data availability statement. This statement should provide the following information, where applicable:

- Accession codes, unique identifiers, or web links for publicly available datasets
- A list of figures that have associated raw data
- A description of any restrictions on data availability

Source data for Figures 1D (histogram), 1E (coverage), 1F (density after adding tau), 1H-(density after removing tau), 2B (decay times), 3C (Tau density change) and Supplementary Figures 1A (nucleations), 1B (growth velocity), 1C (island lengths), 1D (coverage), 1E (coverage after long time), 1F (density change after 30s), 1G (example fits at 0 nM), 1H (disassembly velocity), 1I (fission rate), 2A (binding and unbinding), 2B (20 nM replacement), 2C (100 nM replacement), 2D (decay times), 2E (histogram), 2F (diffusion coefficient), 3A (fast framerate flush out), 3B (saturation), 3C (density vs. density), 4A (velocity), 4B (dwell time), 4C (landing rate), 4D (katanin cutting surrounding), 4E (katanin cutting islands), 4E (island shrink velocity), 4G (Kip3 velocity), 4H (Kip3 landing), 4I (island displacement rate), 5B (intensity after flushout), 5C (line scan, high curvature, SD-Katanin cutting probability), 5G (bend assembly), 5H (density at 20 nM) and quantifications given in main text (island density) have been provided as Supplementary Table 1 (Statistics Source Data). Exemplary raw movies are available at BioStudies (https://www.ebi.ac.uk/biostudies/), accession number S-BSST266. All other data supporting the findings of this study is available from the corresponding authors on reasonable request.

Field-specific reporting

Please select the one below that is the best fit for your research. If you are not sure, read the appropriate sections before making your selection.

☒ Life sciences   ☐ Behavioural & social sciences   ☐ Ecological, evolutionary & environmental sciences

For a reference copy of the document with all sections, see nature.com/documents/nr-reporting-summary-flat.pdf

Life sciences study design

All studies must disclose on these points even when the disclosure is negative.

Sample size	During each independent experiment (in each individual flow chamber) microscopy fields of view were chosen randomly within the flow chambers. In each field of view, a certain number of molecules, islands or microtubules were present, thus determining the sample size per measurement. If experimentally possible (for image acquisition times of ten minutes or shorter), several fields of view per flow channel were imaged.
Data exclusions	No data was excluded.
Replication	Experiments were performed over several months by three independent experimentalists, all replication attempts (that were not impeded by unrelated events, like an image-acquisition software malfunction) were successful. For each quantified experiment and each exemplary image or kymograph 'N' describes the number of either biologically independent samples (individual tau molecules, islands of tau molecules or microtubules, respectively) or the number of independent events (island nucleation, island merging or island fission, respectively). In all cases the number of independent experiments, during which the data was gathered in the course of several days, refers to the number of independent flow chambers, which were assembled, filled with assay components and imaged individually.
Randomization	The allocation of samples into different groups was not required, since one advantage of in vitro experiments is that during one set of experiments all variants but one (for example the concentration of the protein of interest) are kept constant, hence the control of covariants is not relevant to this study.
Blinding	The study did not involve animals and/or human research participants; therefore, investigators were not blinded to the variance in the tested parameters during data collection and analysis. Blinding to group allocation was not relevant to this study (please see above).

Reporting for specific materials, systems and methods

We require information from authors about some types of materials, experimental systems and methods used in many studies. Here, indicate whether each material, system or method listed is relevant to your study. If you are not sure if a list item applies to your research, read the appropriate section before selecting a response.

Materials & experimental systems

n/a	Involved in the study
☐	☒ Antibodies
☒	☐ Eukaryotic cell lines
☒	☐ Palaeontology
☒	☐ Animals and other organisms
☒	☐ Human research participants
☒	☐ Clinical data

Methods

n/a	Involved in the study
☒	☐ ChIP-seq
☒	☐ Flow cytometry
☒	☐ MRI-based neuroimaging

Antibodies

Antibodies used	Biotin antibodies - Sigma B3640, diluted 20 μg/ml in PBS, binding unspecifically to DDS-treated microscopy coverslips, were used to immobilize biotinylated microtubules, in our flow chambers, on these microscopy coverslips.
Validation	In absence of biotin antibodies, the biotinylated microtubules did not bind to the micrososcope surface. Immobilizing the microtubules was the sole purpose of the antibodies, hence, no further tests were performed.